Removal of liver activity contamination in teboroxime dynamic cardiac SPECT imaging with the use of factor analysis

Arkadiusz Sitek, PhD,[a,b] Edward V. R. Di Bella, PhD,[b] Grant T. Gullberg, PhD,[b] and Ronald H. Huesman, PhD[a]

Background. **One of the major problems associated with technetium 99m teboroxime cardiac imaging is the high concentration of activity in the liver. In some cases it is impossible to diagnose defects on the inferior wall because of the finite resolution and scatter that cause images of the inferior wall and the liver to overlap.**

Methods and Results. **The least-squares factor analysis of dynamic structures method, with correction for non-unique solutions, was used to remove the liver activity from the image. The method was applied to dynamically acquired Tc-99m teboroxime data. The liver activity removal method was tested through use of computer simulations and tomographically acquired canine and patient cardiac studies. In all studies the least-squares factor analysis of dynamic structures method was able to extract the liver activity from the series of dynamic images, thereby making it possible to remove it quantitatively from the entire series. The method was used successfully to remove the liver activity that partially overlapped the inferior wall in normal hearts. The method tends to increase the contrast between defects and normal myocardial tissue in abnormal hearts.**

Conclusions. **The method presented can be used to assist in diagnosis of cardiac disease when dynamically acquired teboroxime data are used. Because the contrast between the defect and normal myocardial tissue can be changed, the processed image cannot be used by itself to make an accurate diagnosis. However, with the liver activity removed, the image provides additional information that is very useful in the imaging of patients whose liver activity overlaps the inferior heart wall. (J Nucl Cardiol 2002;9:197–205.)**

Key Words: Teboroxime • dynamic single photon emission computed tomography • liver activity • least-squares factor analysis of dynamic structures

Teboroxime is a neutral, lipophilic agent labeled with technetium 99m that is used for myocardial perfusion imaging.[1] Its very high extraction[2] potentially makes it an excellent perfusion agent for detecting coronary disease with high sensitivity and specificity. Teboroxime results have been shown to be comparable to those of thallium in a small study.[3] The rapid clearance characteristics of teboroxime make it valuable for use in clinical imaging. It has an advantage over thallium in that it enables rapid completion of rest and stress perfusion studies, and the gamma energy of teboroxime is much better suited for imaging than the energy of thallium. The rest-stress studies with teboroxime can be performed within 1 hour of one another, whereas when thallium is used, redistribution imaging is not performed until 3 to 24 hours after the initial injection. However, to establish teboroxime as a clinically useful radiopharmaceutical, the effects of liver uptake must be mitigated or eliminated.

Teboroxime data were acquired differently with the use of fast-rotation single photon emission computed tomography (SPECT).[4-7] A 3-head detector was used for this acquisition protocol. One complete set of tomographic data (360°) was acquired as the camera gantry rotated 120°. This protocol enables the rapid acquisition of complete sets of tomographic data. A continuous rotation was used, with the camera rotating back and forth to acquire multiple 360° acquisitions. One complete set of tomographic data was acquired over 6 to 10 seconds. During the entire teboroxime study, which

From the E. O. Lawrence Berkeley National Laboratory,[a] Berkeley, Calif, and the Radiology Department, University of Utah, Salt Lake City, Utah.[b]

Supported by National Institutes of Health Grant No. ROI HL 50663.
Received for publication April 25, 2001; final revision accepted Aug 20, 2001.

Reprint requests: Arkadiusz Sitek, Radiology Department, Beth Israel Deaconess Medical Center, 330 Brookline Ave, Boston, MA 02215; *asitek@caregroup.harvard.edu.*

1071-3581/2002/$35.00 + 0 **43/1/120362**
doi:10.1067/mnc.2002.120362

lasted approximately 15 minutes, 100 to 200 complete sets of projections were acquired. All tomographic sets were then reconstructed, which resulted in sequences of 100 to 200 dynamic images. The fast-rotation dynamic SPECT protocol is difficult to use, however, because of the camera hardware requirements and computer power needed to store and reconstruct the large amounts of data.

One of the major problems associated with teboroxime imaging is the occurrence of very high liver uptake. Liver activity interference severely affects imaging of the inferior wall of the heart in some patients. In one study, it was reported that severe liver activity interference occurred in 30% of cases when imaging was done 2 to 8 minutes after injection (22 patients evaluated).[8] In another, it was reported that the inferior wall could not be evaluated in 68% of patients.[9] The acquisition protocol was similar and was done 2 to 7 minutes after injection (30 patients were evaluated). Such high probability of liver activity interference on diagnosis makes high liver uptake one of the major problems associated with teboroxime imaging.

The proximity of the liver to the myocardium is responsible for the liver activity interference. This, with finite resolution of SPECT systems, partial volume effects, and Compton scatter, makes the liver appear to overlap the inferior wall in reconstructed images. In some cases the activity in the liver may be several times higher than in the myocardium, especially 5 to 6 minutes after injection. When the physical reasons listed above were taken into account, it was not possible to make a diagnosis of the inferior wall in these cases.

We have developed a technique that will help in the diagnosis of defects of the inferior wall in cases in which there is severe liver activity interference. This is done with factor analysis techniques that separate regions in the image with different temporal behaviors.[10-13] Because the liver has different dynamics of uptake than the myocardium, the factor analysis of dynamic structures (FADS) method can be used to separate the myocardium from the liver. The FADS technique can only be applied to dynamic sequences. A dynamic sequence in SPECT must be acquired either with a fast rotation SPECT protocol (as in this article) or through use of slow rotation acquisition (eg, 20 seconds per projection) with dynamic SPECT reconstruction.[14–17]

METHODS

Factor Analysis

The main assumption made in this article is that the dynamics of the pharmaceutical can be described with a factor model. The factor model of the dynamic data assumes that activity in each pixel is a linear combination of factors ($\tilde{\mathbf{F}}$) with coefficients defined in the matrix ($\tilde{\mathbf{C}}$). On the basis of this assumption the dynamic sequence ($\mathbf{A}$) can be written as follows:

$$\mathbf{A} = \tilde{\mathbf{C}}\tilde{\mathbf{F}} \tag{1}$$

The size of $\mathbf{A}$ is $N \times M$, in which N is the number of pixels in the image and M is the number of dynamic images. The matrix of factors ($\tilde{\mathbf{F}}$) is $K \times M$ and the matrix of factor coefficients is $N \times K$, in which K is the number of factors.

In the factor model it is therefore assumed that the entire organ, or the single physiological region, will have the same dynamics of uptake of the pharmaceutical. So, for example, we expect that the entire volume of the liver, which is in the field of view, will have exactly the same dynamics of wash-in and wash-out of the pharmaceutical.

In the case of teboroxime cardiac imaging, the appropriate regions are the left ventricular blood pool, right ventricular blood pool, myocardium, and liver.

Images of the factor coefficients ($\mathbf{C}$) and factor curves ($\mathbf{F}$) were obtained with the use of penalized least-squares FADS (PLS-FADS).[13,18]

Computer Simulations

Computer simulations were performed with the mathematical cardiac torso (MCAT) phantom.[19] For each time frame, sinograms that consisted of 120 projections (3-head detector, 40 projections for each head) were simulated for each slice. A total of 24 slices of the MCAT phantom were used, and the projection data were rebinned into a 64-pixel matrix. Ninety time frames were simulated, each taken for 10 seconds. Photon attenuation was simulated, and Poisson noise was added to the projections in an amount that resulted in the number of counts in all 24 sinograms (1 for each slice) equal to 4 million. Similar numbers of counts were found in experimental patient studies. Projections were then reconstructed with the use of 25 iterations of the maximum-likelihood expectation maximization[20] algorithm with attenuation correction. The reconstructed dynamic sequences were reoriented to a short-axis view, and the regions of 10 slices (17×17 pixel size) encompassing the heart for each of the 90 temporal views were extracted. The simulated pixel size was 0.6 cm. The entire simulated study lasted 15 minutes.

Dynamically, a total of 5 physiological regions were simulated: the left ventricular blood pool (LV), the right ventricular blood pool (RV), the background, the myocardium (left and right ventricle), and the liver. All of these components (except for the background, which was present in all areas other than the presented factors) are presented in Figure 1. The activity in the LV was simulated as a sum of 3-exponential decay terms with the following function:

$$LV(t) = \begin{cases} 0 & t < 10 \\ 120(t-10)/20 & 10 < t \le 30 \\ 84\exp[-0.1(t-30)] & \\ \quad + 28\exp[-0.014(t-30)] & \\ \quad + 8\exp[-0.00025(t-30)] & t > 30 \end{cases} \tag{2}$$

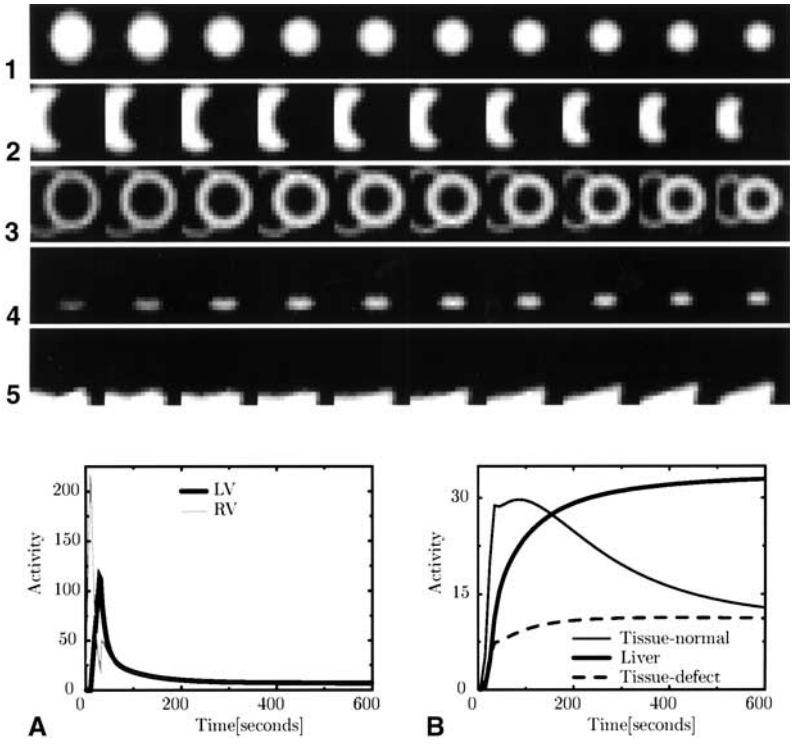

Figure 1. Images of the MCAT phantom used in computer simulations. In each row, images of 10 slices, 16 × 16 pixels in size, are presented. From the top, images of the LV (*row 1*), RV (*row 2*), myocardial tissue (*row 3*), defect (*row 4*), and liver (*row 5*) are presented. The images of the background were simulated in every slice where there were no other components. The graphs represent the simulated time behavior of given components: simulated TACs of the LV and RV **(A)** and TACs of the normal myocardial tissue, liver, and defect (**B**). The TAC of the background was the same as the LV, but the amplitude was one tenth of the LV.

in which t represents the time in seconds. Equation 2 was found to better approximate the input function than the 2 exponential input functions used previously[7,12] in 6 rest-stress patient studies.

Activity in the RV was simulated with the following function:

$$RV(t) = \begin{cases} 240t/10 & t \le 10 \\ 240 \exp[-0.12(t-10)] & 10 < t \le 31 \\ (1 - \exp[-0.07(t-30-t_x)])LV(t) & 31 < t \end{cases} \quad (3)$$

in which $t_x = 1 - 10\ln(LV[31]/[LV(31) - RV(31)])$. It is important to note that both the RV and LV functions are only approximations of the behavior of the functions observed experimentally; they do not have any theoretical basis.

The activities of the myocardium were governed by the 1-compartment model according to the following:

$$M(t) = k_{21}\int_0^t e^{-k_{12}\tau} LV(t-\tau)d\tau + f_v LV(t) \quad (4)$$

in which $M(t)$ and $LV(t)$ are the time behaviors of the myocardium and the left ventricle, respectively. The parameters k_{21} (wash-in), k_{12} (wash-out), and f_v (fraction of blood) were the kinetic parameters of the model and were equal to 0.01 s^{-1}, 0.00667 s^{-1}, and 0.15, respectively, in normal myocardial tissue. In simulations in which the defect in the myocardium was simulated, the abnormal myocardial tissue was simulated by setting k_{21}, k_{12}, and f_v to one fourth of those values that comprise normal myocardial tissue. In the simulations the defect was placed in the inferior wall of the heart (Figure 1). Background activity was simulated as one tenth of the $LV(t)$.

The activity in the liver, $L(t)$, was assumed to follow the 1-compartment model (Equation 4). Using the analyses of liver function from 3 patients at rest, we found that the ratio of k_{21}/k_{12} was 4.14, 5.38, and 4.33. Thus the values of k_{21} = 0.0067 s^{-1} and k_{12} = 0.0013 s^{-1} were used in the computer simulations. All simulated functions of the $LV(t)$, $RV(t)$, $M(t)$, and $L(t)$ are presented in Figure 1.

Intensities of the reconstructed images were compared through use of region of interest (ROI) measurements. The four 24-pixel ROIs were located in 8 slices (3 pixels in each) in the septal, anterior, lateral, and inferior regions of the myocardium,

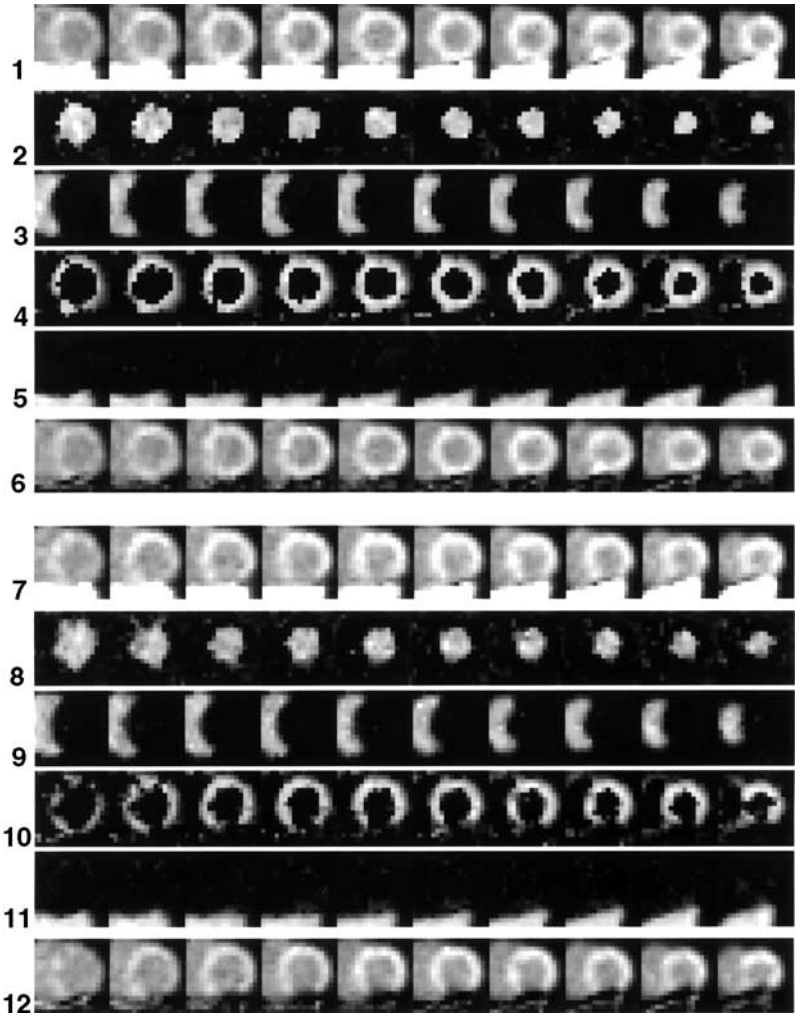

Figure 2. Results of the computer simulation with no defect simulated in the myocardial tissue (*rows 1–6*). *Row 1* is the summed image with the liver close to the inferior wall. The next 4 rows (*2–5*) correspond to the images of factor coefficients extracted by PLS-FADS. These images spatially correspond to the LV, RV, myocardial tissue, and liver, respectively. *Row 6* corresponds to the summed images after the liver activity contamination is removed. The results obtained with the defect simulated in the inferior wall are shown in *rows 7 through 12*. *Row 7* is the summed image. The next 4 rows (*8–11*) correspond to the images of the factor coefficients extracted by PLS-FADS. These images spatially correspond to the LV, RV, myocardial tissue, and liver, respectively. *Row 12* corresponds to the summed images with the liver activity removed.

which will be referred to as ROI_{sep}, ROI_{ant}, ROI_{lat}, and ROI_{inf}, respectively.

Canine Study

A 3-detector camera (PRISM 3000XP; Marconi, Cleveland, Ohio) equipped with fan-beam collimators with focal lengths of 65 cm was used to acquire the data. A transmission scan was performed before emission acquisition with a gadolinium 153 line source. During emission acquisition the camera acquired 180 projections (60 per head) over 360° every 5.7 seconds using continuous movement. The direction of the rotation was changed every 6 seconds. The acquisition was performed for 17 minutes. One hundred seventy-nine sets of tomographic data were then reconstructed with the use of 25 iterations of the maximum-likelihood expectation maximization[20] algorithm with attenuation correction through use of the attenuation maps acquired during the transmission scan. The reconstructed 3-dimensional images were reoriented to obtain short-axis slices. A series of 179 images, each consisting of 8 slices, 13 × 13 pixels in size, were analyzed by PLS-FADS.

Patient Studies

A 3-detector camera (PRISM 3000XP, Marconi) with parallel-hole collimators was used for the acquisition of patient

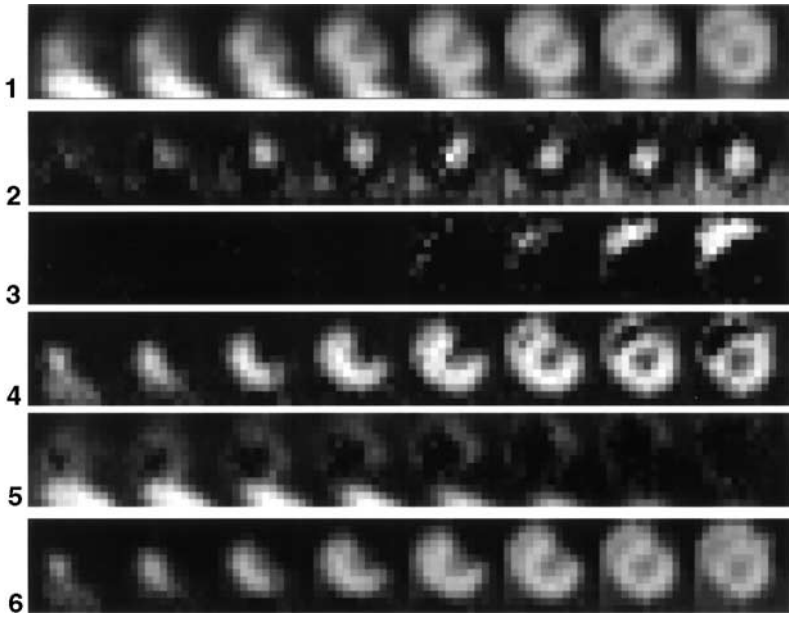

Figure 3. Results of the canine study. The top row (*1*) shows 8 short-axis slices of the summed image with liver interference close to the apex. The next 4 rows (*2–5*) are the factor coefficient images for the LV, RV, myocardial tissue, and liver components, respectively. The final row (*6*) corresponds to the summed image after the liver activity is removed.

data. A transmission scan was performed before the emission acquisition. The results of 2 patient studies are presented. Both were acquired in a rest condition. The patients were injected with a constant 20-second bolus of 17.8 mCi and 22.1 mCi of Tc-99m teboroxime. As in the canine study, consecutive sets of tomographic data (120 projections over 360°) were acquired every 10 seconds, for 15 minutes. A total of 90 images were reconstructed through use of the ordered-subset expectation maximization[21] algorithm (4 iterations, subset size 4) with attenuation and point response corrections. Oblique rotation was applied to the images to obtain short-axis images. A series of images, each consisting of 5 slices, 24 × 22 pixels in size, were analyzed by PLS-FADS in the first patient study. In the second patient study the series of images comprised 7 slices each, 22 × 22 pixels in size, and were analyzed by PLS-FADS. Informed consent for patient studies was obtained.

RESULTS

Results of Computer Simulations

Row 1 in Figure 2 shows the summed image of 78 frames (first 12 frames omitted) with the liver slightly overlapping the inferior wall of the heart. As can be seen in rows 2 through 5 of Figure 2, all 4 components (LV, RV, myocardial tissue, and liver) extracted by FADS from the dynamic sequence accurately resemble the true MCAT components presented in Figure 1. The liver subtraction removes the image of the liver from the summed image. The image is scaled to the activity of the myocardium, but the intensity of the pixels that correspond to the liver (Figure 2, rows 1 and 7) is actually 3 or 4 times greater than that of the myocardial pixels. Liver removal does not change the uniformity of the activity in the myocardium after the subtraction, as shown in row 6 of Figure 2 and in Table 1. This result, however, is based on only one noise realization.

The results of the computer simulations of a heart with defects are presented in Figure 2, rows 7 through 12. Row 7 corresponds to a summed image with an apparent decrease in uptake in the inferior wall, where the defect was simulated. Rows 8 through 11 represent images of factor coefficients extracted by FADS for the LV, RV, myocardial tissue, and liver, respectively. The LV and RV components are very similar to those shown in Figure 1.

The presence of defects affects both the myocardial tissue and liver components. The defect is visible in the images of the myocardial tissue (Figure 2, row 10) and the liver (Figure 2, row 11). The image of the defect is "divided" between the myocardial tissue and the liver components. Row 12 in Figure 2 represents the summed image with the liver activity removed. The contrast between the defect and normal myocardium is increased, as compared with the summed image in row 7.

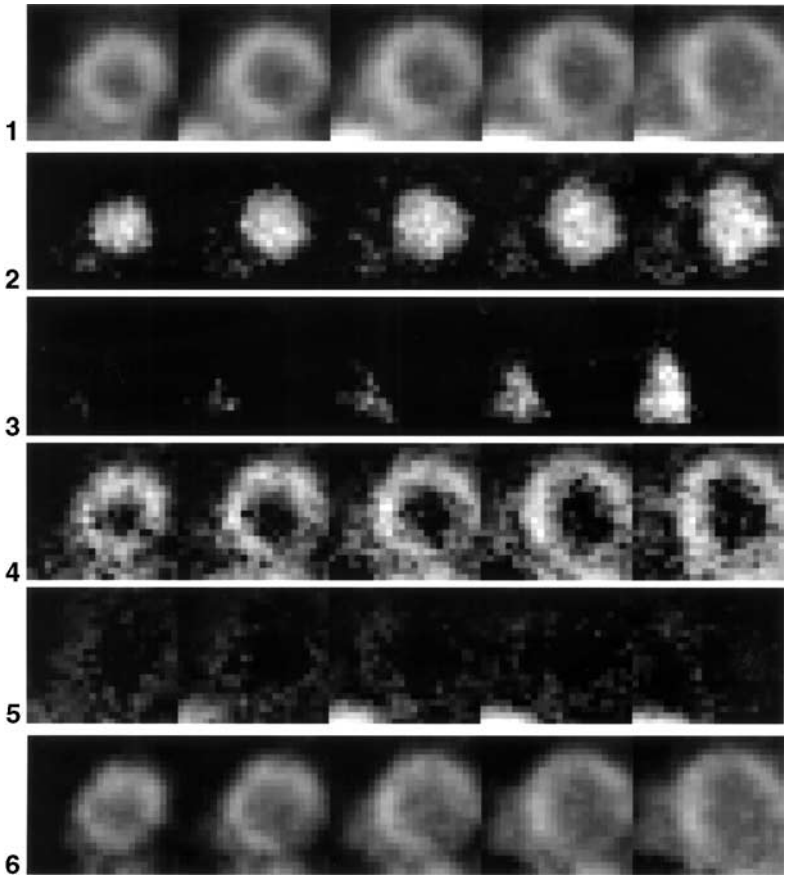

Figure 4. Results of a patient study. The top row (*1*) shows 5 short-axis slices of the summed image. A large defect on the inferior wall can be seen, and a small defect can be seen on the basal exterior-lateral wall. A small amount of liver interference can be seen in the left bottom corner of the basal images. The next 4 rows (*2–5*) show the FADS decomposition into the LV, RV, myocardial tissue, and liver components, respectively. The final row (*6*) shows the summed image with the liver activity contamination removed.

Results of Experimental Studies

Figure 3 presents a summary of the results of the canine study. Row 1 is the summed image of 159 frames (the first 20 frames were omitted). In the apical region of the heart, the liver visibly overlaps the inferior wall. Rows 2 through 5 correspond to images of factor coefficients for the LV, RV, myocardial tissue, and liver, respectively. In the image of the liver (row 5), the shadow of the defect can clearly be seen. After the subtraction of the liver activity from the original sequence in the resulting summed image (Figure 3, row 6), the contrast between the defect and normal myocardial tissue is increased.

In the first patient study, with defects positioned on the inferior wall and basal inferolateral wall, the liver was positioned far from the myocardium, as shown in the summed image in row 1 of Figure 4. The FADS method decomposed the dynamic sequence into 4 factors. The coefficients of these factors are presented in the next 4 rows of Figure 4. It is important to notice that the defect is not visible in the image of the liver (row 5). Therefore

Table 1. Values of intensities in ROIs before and after liver contamination removal for MCAT phantom simulation*

	ROI_{sep}	ROI_{ant}	ROI_{lat}	ROI_{inf}
Normal uptake				
Before	0.99	1.00	1.01	1.06
After	0.94	0.97	1.00	0.96
Abnormal uptake				
Before	0.99	0.94	0.99	0.62
After	0.93	0.90	0.92	0.20

*Values shown are normalized to values obtained in ROIs for computer simulation of MCAT phantom with noiseless data.

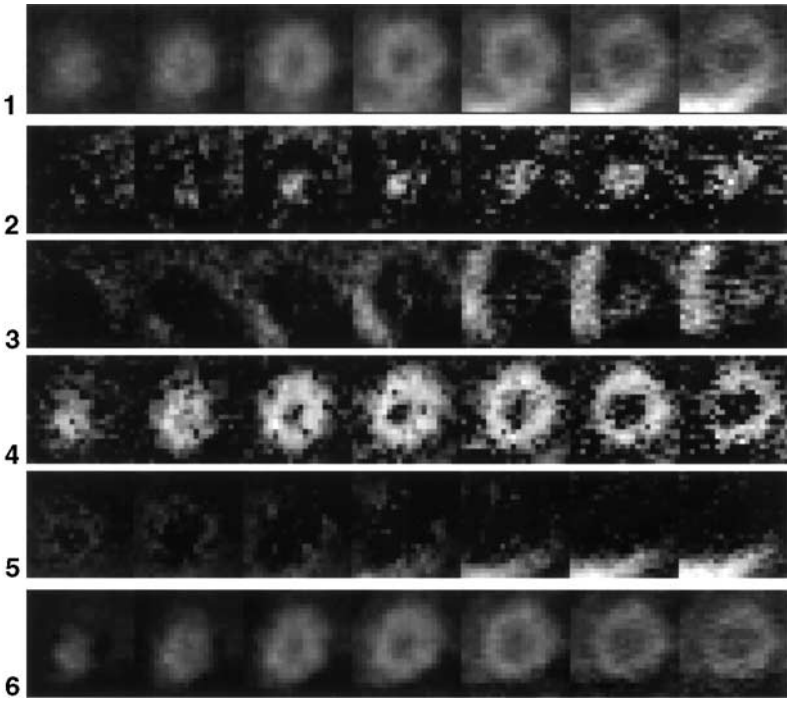

Figure 5. Results of a second patient study. The top row (*1*) shows 7 short-axis slices of the summed image. A large amount of liver interference can be seen in the basal slices that overlap the inferior wall in the region. The next 4 rows (*2–5*) show the FADS decomposition into the LV, RV, myocardial tissue, and liver components, respectively. The final row (*6*) shows the summed image with the liver activity contamination removed.

the liver activity subtraction does not change the contrast between the normal and abnormal myocardial tissues (Figure 4, row 6) as is the case in the computer simulation and the canine study.

In the other patient study, in which the thallium scan appeared normal, the liver interference is severe, which can be seen in the summed image in row 1 of Figure 5. The actual summed activity in the liver is a few times higher than it is in the myocardium, and the liver substantially overlaps the basal inferior wall, making imaging of this wall equivocal. The FADS decomposition results are shown in the next 4 rows of Figure 5. The subtraction of the liver activity completely recovers the image of the inferior wall from the liver interference and only minimally affects other regions in the image, as can be seen in Figure 5.

DISCUSSION

We have presented a technique for removing liver activity contamination from a series of dynamic Tc-99m teboroxime images of the myocardium. It uses a factor analysis technique to identify the liver activity, which is then eliminated from the images. The technique uses a nonstandard least-squares algorithm in the factor analysis step. The selection of this algorithm is important because it takes into account the non-uniqueness of the factor model and corrects for it. Without this correction the results would be much less accurate and it would be impossible to use this approach to remove the liver activity contamination.

As shown in all of the examples presented herein, liver activity can be removed from dynamic sequences. Liver activity removal makes the diagnosis of defects in the inferior wall possible by removing liver overlap, as shown in computer simulations and patient studies (Figures 2 and 5). The problem that must be considered is how the removal of liver activity affects the rest of the image. One answer to this question can be found in the results of the computer simulation. Figure 1 shows that if the myocardium is normal (ie, the dynamics of teboroxime uptake are the same throughout the heart volume), the liver activity is subtracted without any change to the rest of the image (Figure 2, rows 1 and 6). The uniformity of the myocardium is not changed, although the values of the intensities are decreased (Table 1). The decrease is due to noise in the liver component image (Figure 2, row 5), which is then subtracted from the summed image. However, because the liver component image is smoothed before the subtraction, it affects only the value of the intensities

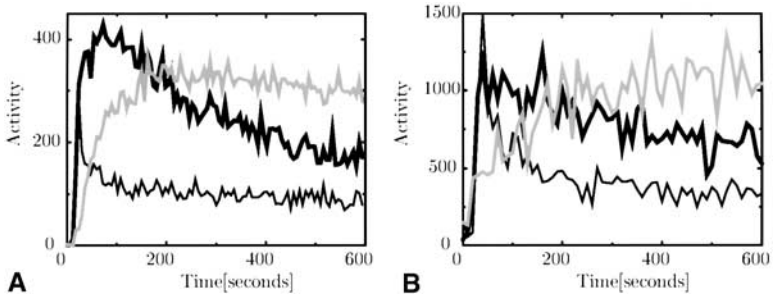

Figure 6. TACs extracted from dynamic sequences with ROI measurements (15-pixel ROI sizes) for a canine study **(A)** and a patient study **(B)**. The *thick black line* corresponds to the myocardial tissue, the *thick gray line* corresponds to the liver, and the *thin black line* corresponds to the defect.

without considerably changing the uniformity of the normal myocardium (ROI_{sep}, ROI_{ant}, and ROI_{lat}).

In the case of a simulated abnormality in the myocardium, the subtraction increases the contrast between the normal and abnormal myocardial tissues (Figure 2, rows 7 and 12). Table 1 shows that the subtraction considerably changes the intensity of ROI_{inf}. The effect can also be seen in the canine study (Figure 3). When factor analysis is performed, this effect occurs because it is assumed that there are only 4 factors in the images. That holds true in the case of a normal study (LV, RV, myocardial tissue, and liver), but in an abnormal case there are 5 different time behaviors in the image (LV, RV, normal myocardial tissue, abnormal myocardial tissue, and liver). Therefore the factor model with 4 components does not adequately represent all of the dynamic changes in cases that involve abnormal myocardial tissue. Consequently, the smallest component (a defect, in the case of cardiac imaging) will be approximated by the linear combination of the other factors. In Figure 1, *B*, the shape of the defect curve is somewhat in between those of the liver and the myocardial tissue, and consequently, the defect partially shows up in the coefficient image of the liver and myocardial tissue in computer simulations and a canine study. Obviously, because the defect shows on the image of the liver, after the subtraction of the liver activity from the original image, the defect will also be subtracted, resulting in an apparent increase in contrast between the images before and after liver activity removal.

The most obvious solution to this would be to use FADS to extract the defect component as well. Five factors could then be used when performing the factor analysis ($K = 5$ in Equation 3 in reference 13). Unfortunately, because of high noise and severe nonuniqueness problems, the extraction of the defect as an additional factor is not possible at the noise levels found in dynamic teboroxime studies with the use of the method described in this article or the use of any other factor analysis methods known to us.

Although an increase in contrast between the defect and normal myocardial tissue was observed in the computer simulations and canine study, this increase was not present in the patient study with the defect. This is because, in the patient study, the time-activity curve (TAC) that corresponded to the defect was more similar in shape to that of the myocardial tissue rather than the liver (Figure 6, *B*). Consequently, the defect did not show up on the image of liver coefficients, and the contrast was not increased after liver activity removal. In Figure 1, *B*, and Figure 6, *A*, the defect TAC more closely resembles the liver TAC, and it follows that it is much more likely that the defect will be present in the image of the liver coefficients, as was observed in the computer simulations and canine study. However, these examples are not significant enough for any strong conclusions to be made. Further investigation involving additional experimental patient data is needed to determine the relationships between the shapes of the TACs for the defect, liver, and normal myocardium and their influence on the results of factor analysis.

In its current state the method can be used for liver activity removal to help in diagnosis of the inferior wall in cases with severe liver interference. It is very important, though, to mention that the image that results from the liver subtraction cannot be used by itself for the diagnosis because, as has been shown in this article, liver removal can change the contrasts between infarcts and healthy myocardial tissue. We believe that with that knowledge in mind, used in conjunction with the original image, the method can provide additional useful information that will be especially important in severe liver interference cases.

One very encouraging fact is that when the myocardium is healthy, the liver removal described in this article does not change any contrasts in the images. The method will affect the image only when there is a differential uptake in the myocardium (abnormalities in the heart). That is why we believe that, although presently a disadvantage, the change of contrasts in the image, due

to application of factor analysis and liver activity removal, might in the future actually help to diagnose abnormalities by improving the contrasts between abnormalities and normal myocardial tissues.

We see a great potential for our method in the analysis of teboroxime data acquired dynamically. We also foresee its application in the detection of abnormalities in the myocardium. With better understanding of the observed tendency to increase the contrast between the normal and abnormal myocardial tissue, this technique could be a great help in myocardial diagnosis. In addition, we plan to extend the method and apply it to static studies.

In summary, we have presented a technique based on factor analysis to remove liver activity contamination from a dynamic series of cardiac Tc-99m teboroxime images. The PLS-FADS algorithm that corrects for nonuniqueness effects of a factor model was used. The method was tested in computer simulations with an MCAT phantom; abnormalities in the myocardium were simulated. Liver activity removal was also tested in an experimental canine study and patient studies. It was found that the technique worked well in all studies. The liver activity interference was removed from the dynamic series of images. In some cases, liver activity removal tended to increase the contrast between the abnormal and normal myocardial tissue in the heart, which was observed in the computer simulations and canine study, but not in the patient studies.

Acknowledgment

We would like to acknowledge Sean Webb for proofreading the manuscript.

The authors have indicated they have no financial conflicts of interest.

References

1. Narra RK, Nunn AD, Kuczynski BL, Feld T, Wedeking P, Eckelman WC. A neutral technetium-99m complex for myocardial imaging. J Nucl Med 1989;30:1830-37.
2. Leppo JA, Meerdink DJ. Comparative myocardial extraction of two technetium-labeled BATO derivatives (SQ30217, SQ32014) and thallium. J Nucl Med 1990;31:67-74.
3. Leppo JA, DePuey EG, Johnson LL. A review of cardiac imaging with sestamibi and teboroxime. J Nucl Med 1991;32: 2012-21.
4. Smith AM, Gullberg GT, Christian PE, Datz FL. Kinetic modeling of teboroxime using dynamic SPECT imaging of a canine model. J Nucl Med 1994;35:484-95.
5. Chiao P-C, Ficaro EP, Dayanikli F, Rogers WL, Schwaiger M. Compartmental analysis of technetium-99m-teboroxime kinetics employing fast dynamic SPECT at rest and stress. J Nucl Med 1994;35:1256-73.
6. Smith AM, Gullberg GT, Christian PE. Experimental verification of technetium 99m-labeled teboroxime kinetic parameters in the myocardium with dynamic single-photon emission computed tomography: reproducibility, correlation to flow, and susceptibility to extravascular contamination. J Nucl Cardiol 1996;3:130-42.
7. Gullberg GT, Huesman RH, Ross SG, Di Bella EVR, Zeng GL, et al. Dynamic cardiac single-photon emission computed tomography. In: Zaret BL, Beller GA, eds. Nuclear cardiology. state of the art and future directions. Mosby: St. Louis, 1999: 137-87.
8. Bontemps L, Geronicola-Trapali X, Sayegh Y, Delmas O, Itti R, Andre X. Technetium-99m teboroxime scintigraphy. Clinical experience in patients referred for myocardial perfusion evaluation. Eur J Nucl Med 1991;18:732-39.
9. Chua T, Kiat H, Germano G, Takemoto K, Fernandez G, Baisio Y, et al. Rapid back to back adenosine stress/rest technetium-99m teboroxime myocardial perfusion SPECT using a triple-detector camera. J Nucl Med 1993;34:1485-93.
10. Di Paola R, Bazin JP, Aubry F, Aurengo A, Cavailloles F, Herry Y, et al. Handling of dynamic sequences in nuclear medicine. IEEE Trans Nucl Sci 1982;NS29:1310-21.
11. Benali H, Buvat I, Frouin F, Bazin JP, Di Paola R. A statistical model for the determination of an optimal metric in factor analysis of medical sequences (FAMIS). Phys Med Biol 1993; 38:1065-82.
12. Sitek A, Di Bella EVR, Gullberg GT. Factor analysis with a priori knowledge—application in dynamic cardiac SPECT. Phys Med Biol 2000;45:2619-38.
13. Sitek A, Gullberg GT, Huesman RH. Correction for ambiguous solutions in factor analysis using a penalized least squares objective. In: 2000 IEEE Nuclear Science Symposium and Medical Imaging Conference Record. Lyon, France: October 15–20, 2000. p. 2292-6.
14. Limber MN, Celler A, Barney JS, Limber MA, Borwein JM. Direct reconstruction of functional parameters for dynamic SPECT. IEEE Trans Nucl Sci 1995;42:1249-56.
15. Celler A, Farncombe T, Bever JM, Noll D, Maeght J, Harrop R, et al. Performance of the dynamic single photon emission computed tomography (dSPECT) method for decreasing or increasing activity changes. Phys Med Biol 2000;45:3525-43.
16. Sitek A, Di Bella EVR, Gullberg GT. Reconstruction from slow rotation dynamic SPECT using a factor model. In: Kuba A, Samal M, Todd-Pokropek A, eds. Lecture notes in computer science 1613. Information processing in medical imaging. proceedings of the 16th international conference. Springer: Berlin, 1999. p. 436-41.
17. Sitek A, Gullberg GT, Di Bella EVR, Celler A. Reconstruction of dynamic renal tomographic data acquired by slow rotation. J Nucl Med 2001;42:1704-12.
18. Sitek A, Gullberg GT, Huesman RH. Correction for ambiguous solutions in factor analysis using a penalized least squares objective. IEEE Trans Med Imaging 2002. (In press.)
19. Tsui BMW, Terry JA, Gullberg GT. Evaluation of cardiac cone-beam SPECT using observer performance experiments and ROC analysis (In press). Invest Radiol 1993;28:1101-28.
20. Shepp LA, Vardi Y. Maximum likelihood reconstruction for emission tomography (In press). IEEE Trans Med Imaging 1982; 1:113-22.
21. Hudson HM, Larkin RS. Accelerated image reconstruction using ordered subsets of projection data (In press). IEEE Trans Med Imaging 1994;13:601-9.